ISSN 1063-7729, Astronomy Reports, 2010, Vol. 54, No. 5, pp. 375–385. © Pleiades Publishing, Ltd., 2010.
Original Russian Text © V.V. Bruevich, A.S. Gusev, S.A. Guslyakova, 2010, published in Astronomicheskiĭ Zhurnal, 2010, Vol. 87, No. 5, pp. 419–429.

UBVRI CCD Photometry of the Nearby Low-Surface-Brightness Galaxy NGC 5585

V. V. Bruevich[1], A. S. Gusev[1], and S. A. Guslyakova[1,2]

[1] *Sternberg Astronomical Institute, Moscow State University, Moscow, Russia*
[2] *Space Research Institute, Russian Academy of Sciences, Moscow, Russia*

Received November 12, 2009; in final form, November 26, 2009

Abstract—The structure and composition of the stellar population in the low-surface-brightness galaxy NGC 5585 is studied using $UBVRI$ CCD photometry. The observations were obtained on the 1.5-m telescope of the Maidanak Observatory of the Astronomical Institute of the Academy of Sciences of Uzbekistan under conditions with seeing $1.2''-1.8''$. A two-dimensional decomposition of the galaxy emission into bulge and disk components is carried out. Both components have low surface brightnessess. The Sersic parameter for the bulge is $n = 1.2-1.6$. The effective radius of the bulge in R and I is equal to the scale length for the brightness decrease in the disk, and comprises $30''-40''$ (0.8–1.1 kpc). The spiral arms seem to form a bar, but the centers of the bar and ring do not coincide with the center of NGC 5585. A powerful star-forming region is observed $3.2''$ (100 pc) from the galactic center, whose radiation swamps the nucleus in the U and B filters. Based on the positions of the various components of the galaxy in two-color diagrams, it is concluded that NGC 5585 has a complex star-forming history that may be different at different distances from the center.

DOI: 10.1134/S106377291005001X

1. INTRODUCTION

NGC 5585 is among the most interesting nearby galaxies, and worthy of detailed study. It is a nearby, relatively small (see Table 1) galaxy with a low surface brightness, with more than 80% of its mass being comprised of dark matter [1]. It is classified as an SABc (LEDA) or SAB(s)d (NED) galaxy, and has a non-trivial morphology (Fig. 1). Based on the results of $BVRI$ aperture photometry, Hernandez-Toledo and Ortega-Esbri [2] identified and determined the parameters of a small bar and a fragment of one (the only) spiral arm in the galaxy; however, the bar of NGC 5585 was not detected in the infrared observations of [3].

The photometric characteristics of NGC 5585 are typical for extremely late-type galaxies (Sd–Sm–Im) [2]. Active star formation is observed in the galactic nucleus (according to the spectrophotometric data of [4]).

Numerous HII regions have been found in NGC 5585 [5–7], as well as five supernova remnants [8]. However, no molecular hydrogen has been detected in the galaxy ($M(\mathrm{H_2}) < 1.3 \times 10^7\ M_\odot$ based on CO line observations) [9]. Nevertheless, the total mass of gas ($1.4 \times 10^9\ M_\odot$) exceeds the total mass in stars ($1 \times 10^9\ M_\odot$) in NGC 5585 [10].

The question of the distance of NGC 5585 warrants a separate discussion. Adopted distances in the literature vary from 5.7 Mpc [11] to 10.5 Mpc [4]. Here, we use the value 5.7 Mpc, which is based on photometry of the brightest stars in the galaxy [11].

The specific properties of the morphology, kinematics, and star-formation history in NGC 5585 may be associated with interactions and mergers of galaxies. Although NGC 5585 is not currently interacting and has no neighbors with comparable mass [2], it is a member of the group M 101 [12] and has several dwarf satellites [2].

The properties of NGC 5585 make it a dwarf low-surface-brightness galaxy [9, 13]. The galaxy's luminosity is $L_B = 1.5 \times 10^9 L_\odot$, with $M_*/L_B = 1.0(M/L)_\odot$ [10]. The total mass of the galaxy at $r = 6.5$ kpc (the Holmberg radius) is $1.1 \times 10^{10}\ M_\odot$ with $M/L_B = 10.1\ (M/L)_\odot$ [10]. Thus, dark matter dominates everywhere in the galaxy, except for the circumnuclear region [1]. Note, however, that, in contrast to most dwarf low-surface-brightness galaxies, active star formation is ongoing in the nucleus and disk of NGC 5585.

The goal of the current study is a photometric and morphological analysis of the properties of NGC 5585, the composition of the stellar population, and regions of ongoing star formation in the

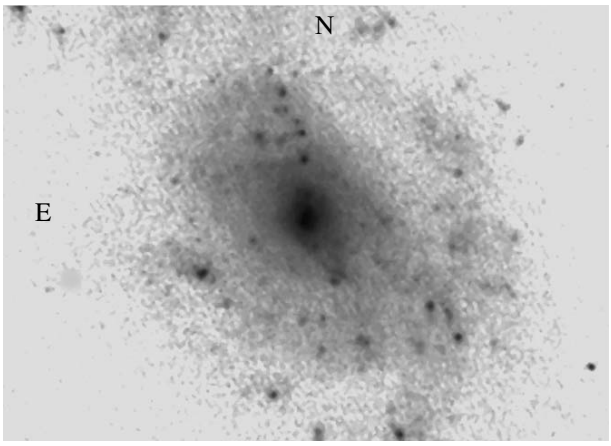

Fig. 1. Image of NGC 5585 in the B filter. The size of the image is $4.1' \times 3.1'$. North is up and East is to the left.

galaxy. No previous multi-color surface photometry of NGC 5585 has been published. Previous photometric observations have been aimed at studying star-forming regions in the galaxy [5, 6]. The studies of Hernandez-Toledo and Ortega-Esbri [2] were based on $BVRI$ aperture photometry.

Table 1. Main characteristics of the galaxy

Parameter	Value	Source
Type	SABc	LEDA
m_B, mag	11.39	LEDA
$M_B^{0,i}$, mag	−18.48	LEDA
V_{Vir}, km/s	573	LEDA
R, Mpc	5.7	[11]
D_{25}, arcmin	4.27	LEDA
D_{25}, kpc	7.1	LEDA, [11]
i, deg	53.2	LEDA
b/a	0.62	LEDA
P.A., deg	34.2	LEDA
V_{max}^{rot}, km/s	79.1	LEDA
$A(B)_0$, mag	0.07	LEDA
$A(B)_i$, mag	0.38	LEDA
$(U-B)_0^i$	−0.26	LEDA
$(B-V)_0^i$	0.40	LEDA
$(V-R)_0^i$	0.40	[2]
$(V-I)_0^i$	1.04	[2]

The main parameters of the galaxy (from the LEDA database) are presented in Table 1.

2. OBSERVATIONS AND DATA REDUCTION

The observations were obtained in September 2005 on the 1.5-m telescope of the Maidanak Observatory (Institute of Astronomy of the Academy of Sciences of Uzbekistan), which has a focal length of 12 m, using a SITe-2000 CCD array. With broadband U, B, V, R, and I filters, this CCD array realizes a photometric system close to the standard Johnson–Cousins $UBVRI$ system. The array was cooled with liquid nitrogen. The size of the array is 2000×800 pixels, providing a $8.9' \times 3.6'$ field of view with an image scale of $0.267''$/pixel. An observing log is presented in Table 2.

The subsequent reduction of the data was carried out at the Sternberg Astronomical Institute (SAI) of Moscow State University using the standard procedures in the ESO-MIDAS image-reduction system. The main reduction steps included flat fielding and correction for the CCD bias; removal of cosmic-ray traces; subtraction of the sky background for each image; superposition of the galaxy images using reference stars; addition of the galaxy images made in a single filter; translation of the counts to a logarithmic scale (magnitudes per square arcsecond) using the results of photometric calibration; corrections for differences of the instrumental photometric system from the standard Johnson–Cousins system and the air mass (allowing for the obtained color equations and aperture photometry of the galaxy); and subtraction of the galaxy images made in different filters in order to obtain color-index maps.

To construct the color equations and correct for atmospheric extinction, we used observations of the Landolt [14] standard fields of stars SA113 and SA92

Table 2. Observing log

Date	Filter	Exposure, s	Air mass $M(z)$	Seeing, arcsec
September 8/9, 2005	U	3×360	1.54–1.60	1.62–1.81
	B	4×180	1.65–1.71	1.52–1.57
	R	2×120	1.48–1.49	1.26–1.32
	I	2×90	1.50–1.51	1.15–1.29
September 9/10, 2005	U	3×300	1.68–1.73	1.77–1.93
	B	4×180	1.59–1.64	1.62–1.76
	V	2×180	1.53–1.54	1.51–1.61
	R	2×120	1.56–1.57	1.54–1.59
	I	$1 \times 20, 4 \times 90$	1.76–1.82	1.16–1.44

obtained on the same night in the U, B, V, R, and I filters at air masses $M(z) \equiv \sec z = 1.27$–$1.31$. The resulting instrumental *ubvri* system was close to the standard Johnson–Cousins photometric *UBVRI* system, to within 0.022^m in B, V, R, and I and to within 0.074^m in U.

We also compared the data obtained with the results of aperture photometry of the galaxy (data from the LEDA electronic catalog). The accuracy of the photometric tie was 0.02^m in B, 0.015^m in V, and 0.01^m in I. The uncertainty in the zero point for U and R is estimated to be 0.11^m.

All the data (brightnesses and color indices) were corrected for galactic absorption (data from the LEDA database; Table 1) and extinction due to the inclination of the galaxy. We assumed a Hubble constant of $\mathrm{H_0} = 75\ \mathrm{km\,s^{-1}Mpc^{-1}}$. The image scale was 27.6 pc/arcsec.

3. ANALYSIS OF PHOTOMETRY RESULTS

3.1. Determination of the Position Angle and Inclination of the Galactic Disk

The position angle (P.A.) and ellipticity of the galaxy isophotes ($e \equiv 1 - b/a$) were determined using the surfphot library in the MIDAS system. The dependences of the position angle and ellipticity on the distance r from the center of NGC 5585 are presented in Fig. 2.

Note that NGC 5585, with its weak disk and irregular spiral structure, is a complex object for determining P.A. and e, especially in the U filter (Fig. 2b). The integrated values for P.A. and the disk inclination i obtained by various authors differ considerably (see, for example, the LEDA database and [13]).

According to our data, the position angle of the major axis of the galaxy grows smoothly from 20° at $r = 10''$ to 40° at $r = 80''$; in shorter-wavelength bands, P.A. reaches values of 40°–45° at smaller distances r from the center (Fig. 2a). This may indicate the presence of an appreciable spherical relative older stellar component in the galaxy.

The ellipticity of the galaxy isophotes grows from 0.2 at the center to 0.3–0.4 at $r = 60''$, with e being higher in the "bluer" bands (Fig. 2b). This can be explained by peculiarities of the spiral pattern of NGC 5585. In contrast to most galaxies, the ellipticity of the isophotes differs strongly from zero in the central region. The reason for this is the presence of a bright blue condensation near the galactic nucleus. The structure of the central region of NGC 5585 will be considered in more detail below.

Our integrated isophotal position angle and ellipticity are P.A. $= 42° \pm 2°$ and $e = 0.38 \pm 0.03$ (which corresponds to a disk inclination of $i = 52° \pm 2°$).

Figure 3 presents our azimuthally averaged photometric profiles of the galaxy in the U, B, V, R, and I filters obtained in elliptical apertures in steps of $2''$. The shape of these profiles is fairly typical for spiral galaxies, but the surface brightness of NGC 5585 is roughly 2^m weaker than for normal spiral galaxies. Note also the extremely blue center (within $7''$–$8''$), characteristic of galaxies with powerful circumnuclear star formation.

3.2. Decomposition of the Galaxy Emission into Bulge and Disk Components

The decomposition of the galaxy into an exponential disk and a bulge with a previously unknown

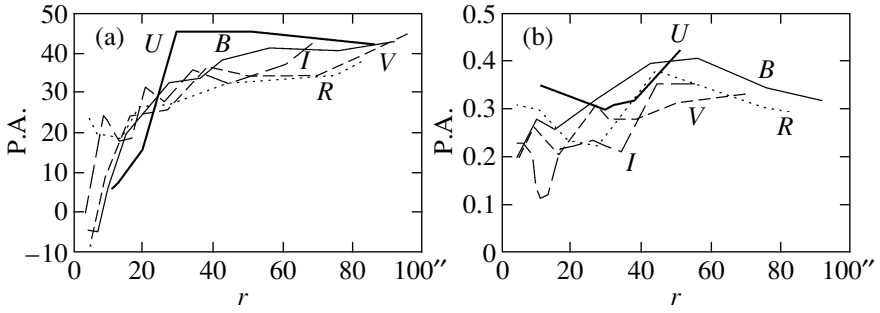

Fig. 2. Dependence of the (a) position angle and (b) ellipticity on the distance r from the center of the galaxy in the U (bold), B (thin), V (short-dashed), R (dotted) and I (long-dashed) filters.

Sersic parameter was carried out using the GalFit program [15]. This program minimizes the difference between the input image and the model, yielding the parameters of the best-fit disk and bulge.

The input parameters for the program are the radial scale of the disk, the radius of the bulge, the position angle and axial ratio for the bulge and disk, the integrated magnitudes of the disk and bulge, the Sersic parameter (which is varied by the program), a parameter characterizing the shape of the isophotes ($x < 0$ for disky and $x > 0$ for boxy isophotes), and the coordinates of the centers of the disk and bulge. Each of these parameters can be fixed if desired.

Since the parameter x is very different for the models in different filters, we decided to approximate the isophotes as ideal ellipses, fixing $x = 0$. We also fixed the size of the region in which the image was convolved with the point spread function. Table 3 presents the results of analyzing the galaxy images with GalFit. We fixed a number of parameters for the images in some filters, since otherwise the program gave clearly incorrect results. This is apparently associated with high noise levels, as, for example, in the I filter, or small signal-to-noise ratios, as in the U filter. These cases are marked in Table 3 with an "f." In this table, R^d is the radial scale length of the disk brightness, μ_0^d the central surface brightness of the disk, R^b the radius of the bulge ($I = I_0 \exp[-(r/R^b)^{1/n}]$), m_0^b the integrated apparent magnitude of the bulge, n the Sersic parameter, and R_{eff}^b the effective radius of the bulge. The "residual" image in B (i.e., after subtracting the model from the input image) is presented in Fig. 4.

A one-dimensional decomposition for NGC 5585 is presented in [16]. According to these data, the disk

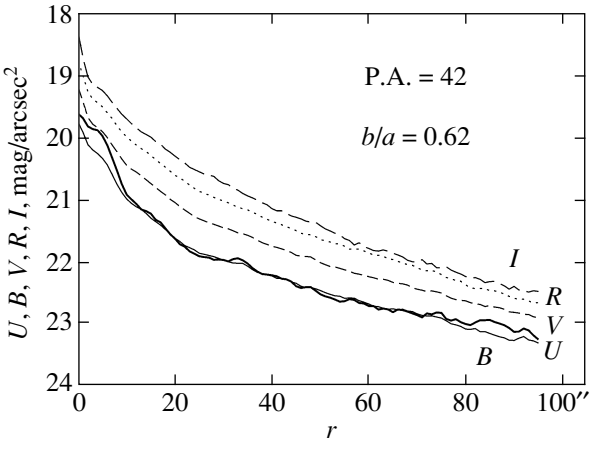

Fig. 3. Azimuthally averaged photometric profiles of the galaxy in the U, B, V, R, and I filters.

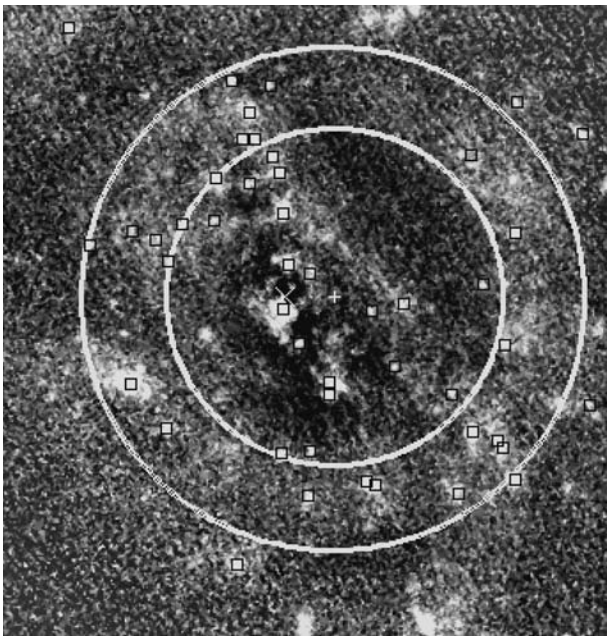

Fig. 4. "Residual" image of the galaxy in the B filter. The size of the image is $3.1' \times 3.1'$. The edge of a ring of star formation in the galaxy with $r_{in} = 50''$, $r_{out} = 75''$, and its center (plus) located $11''$ to the west of the galactic center (x) is shown. The hollow squares show identified star-forming regions in the galaxy.

Table 3. Parameters of the disk and bulge

Filter	R^d, arcsec (R^d, kpc)	μ_0^d, mag/arcsec^2	R^b, arcsec (R^d, kpc)	m_0^b, mag	n	R^b_{eff}, arcsec (R^b_{eff}, kpc)
U	64.67 ± 0.37	22.76	20.28 ± 0.12	13.35 ± 0.01	1.64f	119.6 ± 0.7
	(1.78 ± 0.01)		(0.56 ± 0.00)			(3.30 ± 0.02)
B	62.03 ± 0.23	22.26	16.50 ± 0.22	13.85 ± 0.02	1.60 ± 0.02	89.1 ± 5.2
	(1.71 ± 0.01)		(0.46 ± 0.01)			(2.46 ± 0.14)
V	57.07 ± 0.19	21.73	15.81 ± 0.18	13.31 ± 0.01	1.44 ± 0.01	60.9 ± 2.0
	(1.58 ± 0.01)		(0.44 ± 0.01)			(1.68 ± 0.06)
R	40.7 ± 0.08	20.93	12.29 ± 0.11	13.32 ± 0.01	1.24 ± 0.01	31.8 ± 0.6
	(1.12 ± 0.00)		(0.34 ± 0.00)			(0.88 ± 0.02)
I	39f	20.83	15.71 ± 0.10	12.65 ± 0.01	1.2f	37.6 ± 0.2
	(1.08)		(0.43 ± 0.00)			(1.04 ± 0.01)

scale length in the R filter is $R^d = 41.7'' \pm 1.5''$, in good agreement with our results. Note, however, that, in the opinion of the authors of GalFit, the errors provided by this program may be somewhat underestimated. As in [15], it is suggested that, in order to obtain a correct decomposition, the size of the processed part of the image should be three to five times larger than the visible size of the galaxy. However, this is not possible in the case of NGC 5585, since its angular size is larger than the field of view of the CCD array.

The obtained disk parameters (absolute and relative scale lengths and central surface brightnesses in the various photometric bands) are fairly typical for dwarf late-type galaxies [17]. A diminished central surface brightness is observed for the disks of such galaxies, with $R^d(B)/R^d(I) = 1.2$–1.7, and the linear scales (kpc) for the disk brightness decrease are short, while the relative scales (R^d/D_{25}) are normal or longer than average [17].

The bulge parameters for NGC 5585 are determined with less certainty (Table 3). This is due to the relatively small contribution the bulge makes to the total luminosity of the galaxy in all bands (9–10%), as well as the presence of a circumnuclear region of star formation, which influences the bulge parameters in short-wavelength bands. The color characteristics of the bulge derived using GalFit are very tentative: we will show below that the real $U-B$ color index in the bulge region is "redder" (because young, massive stars dominate the luminosity in the U filter). However, our derived size ($R^b_{eff}(I) = 1.3$ kpc) and Sersic parameter ($n = 1.2$–1.6) of the bulge are standard for Sc galaxies [18]. Note that, while the bulge of NGC 5585 is not prominent visually in images of the galaxy (Figs. 1, 4), it does exist and makes an appreciable contribution (compared to other late-type galaxies) to the total luminosity, and is fairly extended (we have $R^b_{eff} \approx 0.5R^d_{eff} \approx R^d$ in V, R, I). At the same time, the mean surface brightness of the bulge is low, even compared to the low-luminosity disk of the galaxy.

3.3. Brightness and Color Distribution, Structure of the Galaxy

Photometric profiles along the major axis of the galaxy and maps of the B isophotes are presented in Figs. 5a and 5b, and profiles and maps of the $U-B$ and $B-V$ color indices in Figs. 6a–6c.

The galactic nucleus is very blue, with color indices of $U-B = -0.25 \pm 0.06$, $B-V = 0.48 \pm 0.07$, $V-R = 0.43 \pm 0.05$, and $R-I = 0.31 \pm 0.16$ (Fig. 6a).

One peculiarity of the galaxy is the presence near the center of a very blue object—a giant star-forming region located $3.2''$ (100 pc) to the South-Southeast of the nucleus, whose bright emission in the U and B bands swamps the light of the nucleus (Fig. 7). The color indices are quite characteristic of a star-forming region, comprising $U-B = -0.57 \pm 0.06$, $B-V = 0.34 \pm 0.03$, $V-R = 0.32 \pm 0.06$, and $R-I = 0.22 \pm 0.18$ in the central part. Precisely this object is responsible for the pronounced asymmetry in the cross section of the galaxy image along the major axis in short-wavelength filters (U and B; Figs. 5a and 6a).

The bulge is the reddest region of the galaxy: $U-B = 0.13 \pm 0.11$, $B-V = 0.58 \pm 0.07$, $V-R = 0.45 \pm 0.06$, and $R-I = 0.30 \pm 0.08$ (Figs. 5a, 6a, 6c).

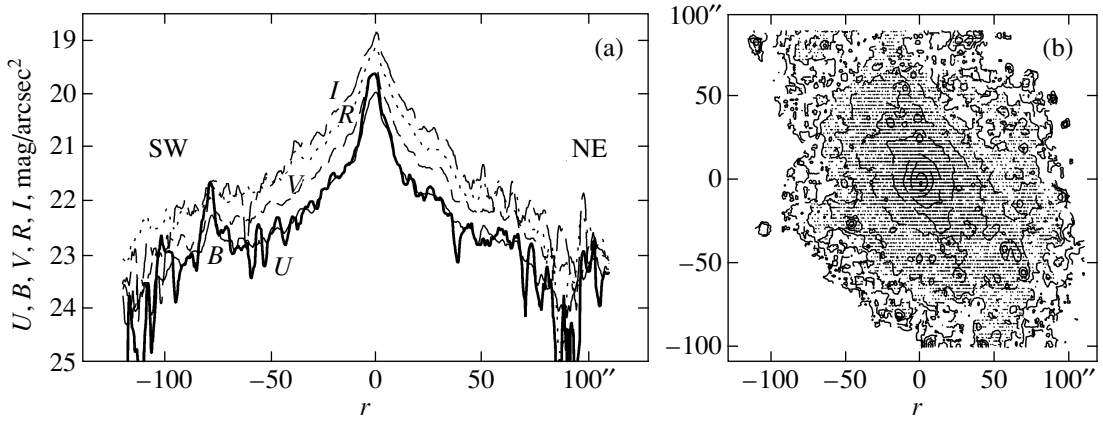

Fig. 5. (a) Photometric profiles along the major axis of the galaxy in the U (bold), B (thin), V (short-dashed), R (dotted), and I (long-dashed) filters. Negative coordinates correspond to the southwest direction from the center. (b) Images of the galaxy in the B filter; the 20.0, 20.5, 21.0, 21.5, 22.0, 22.5, 23.0, 23.5, 24.0, and 24.5 mag/arcsec^2 isophotes are shown.

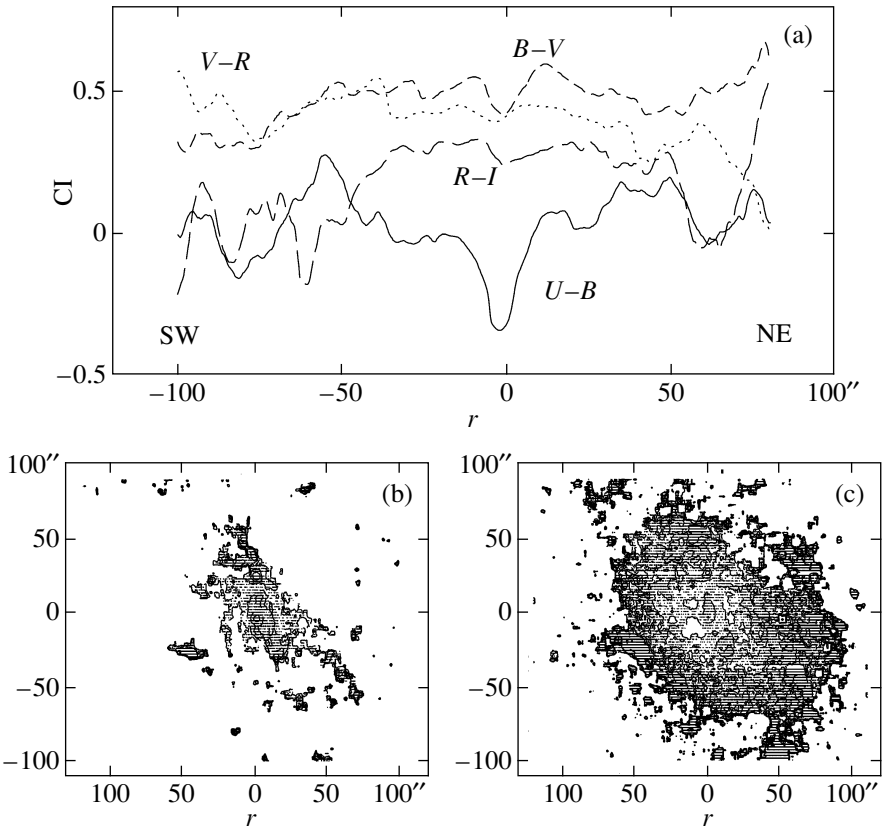

Fig. 6. (a) $U-B$ (solid), $B-V$ (short-dashed), $V-R$ (dotted), $R-I$ (long-dashed) color indices along the major axis of the galaxy. (b, c) Maps of the $U-B$ and $B-V$ color indices; contours of $U-B = -0.4^m$, -0.2^m, 0.0^m, 0.2^m and $B-V = 0.3^m$, 0.4^m, 0.5^m, 0.6^m, 0.7^m are shown (redder regions correspond to lighter regions in the maps).

The relatively low signal-to-noise ratio in U hinders accurate measurement of $U-B$ for the disk. In $B-V$, the disk becomes slightly bluer towards the periphery, decreasing from 0.59 ± 0.01 to 0.50 ± 0.10; $V-R$ varies from 0.46 ± 0.09 to 0.31 ± 0.12; $R-I$ remains essentially constant at 0.33 ± 0.15. Another interesting feature of the galactic disk is that, in most galaxies, $V-R$ for the disk varies only weakly with radius, while the other color indices decrease toward the disk periphery. We see another pattern in NGC 5585: the radial decrease in $V-R$ is the same as for $B-V$ (Fig. 6a).

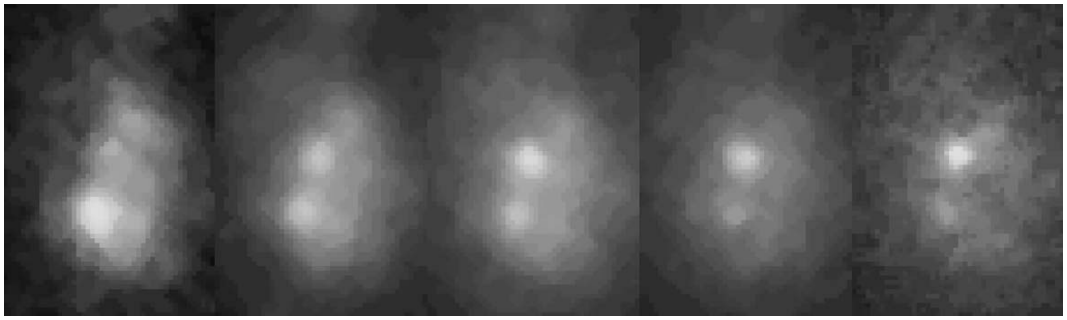

Fig. 7. Image of the central part of the galaxy in U, B, V, R, and I (left to right). The size of the images is $12'' \times 18''$.

The remnants of the galactic spiral arms are too weak to be able to measure them accurately, and are manifest visually only as a collection of bright points that represent star-forming regions extended in a chain. We counted three spiral arms in the galaxy: northern, southwestern, and southern (Fig. 4). We estimate the mean surface brightness of the arms outside regions of star formation to be $22.4^m \pm 0.2^m/\text{arcsec}^2$ in B (Figs. 5a, 5b). Space images show a clearly visible enormous ring framing the galaxy. Unfortunately, the high noise level hindered detection of this ring in our frames, although the residual image shows a fairly large number of regions located nearly along a circular arm at the periphery ($r = 50''-70''$ (1.4–1.9 kpc from the center of the galaxy; Fig. 4). The geometrical center of the ring is offset by $11''$ (300 pc) to the west of the center of NGC 5585 (Fig. 4). NGC 5585 also displays several very bright regions to the northeast of the center, but these are not visible in our images, since they do not fall within the modest field of view of the CCD array.

Figure 4 shows a bar with P.A. $= 40°$ and mean brightness $22.3^m \pm 0.3^m/\text{arcsec}^2$ in the B filter (Fig. 5b). The ends of the (pseudo) bar are in contact with the ring of the galaxy, and powerful regions of star formation are located at the intersection of the (pseudo) bar and ring (Fig. 4). This formation could be taken to be a classical galactic (pseudo) bar if it passed through the center of the galaxy. However the center of the bar-like structure is offset $20''$ (0.6 kpc) to the northwest of the nucleus (Fig. 4).

The U and B images of the galaxy (Figs. 1, 4, 6b) show that the spiral arms of NGC 5585 are wound in different directions: the northern arm in one direction and the two southern arms in the other. The morphology and colors of the galaxy suggest that this may be the result of a galaxy merger. We will consider this question in more detail below.

3.4. Two-color Diagrams

Figure 8 shows the positions of various regions in NGC 5585 on $(U-B)-(B-V)$, $(B-V)-(V-R)$, and $(B-V)-(V-I)$ two-color diagrams. The bold lines indicate the normal integrated color sequence (NCS) of galaxies according to the data of [19]. The numbers denote the following regions: (1) the nucleus (within $r = 1.5''$ (40 pc) of the center), (2) the circumnuclear blue condensation (measured in a $3.2''$ aperture (90 pc), (3) the bulge region at $r = 7''-24''$ (190–660 pc), (4) the disk, (5) the spiral arms, and (6) the ring (Fig. 4). The thin lines indicate how the points on the diagrams would be shifted for absorption by $A(V) = 1^m$ (upward and to the left).

Most of the galactic components lie along the NCS, testifying to a smooth star-formation history in these regions (without powerful bursts of star formation). The ring of NGC 5585 is an exception. The difference between the color characteristics of the nucleus and spiral arms, and even between the bulge and disk, is very small. In spite of the fact that the bulge of NGC 5585 is the reddest region of the galaxy, its photometric characteristics are typical for the disks of spiral galaxies, i.e, for stellar systems with ongoing star formation.

Several galactic components can be distinguished from their positions in two-color diagrams. The bulge and disk have photometric characteristics typical for the disks of Sb spiral galaxies. Strong Hα emission is probably observed in the disk (causing $V-R$ for the disk to become very small; Fig. 8b).

The nucleus and spiral arms have, on average, a relatively younger stellar population, and the color characteristics of these regions are typical for very-late-type spiral galaxies. Based on their position in the two-color diagrams, these are stellar systems with a roughly constant star-formation rate.

The photometric characteristics of the circumnuclear blue condensation suggest it is a region of current star formation. Its parameters will be considered in more detail below, in the section concerned with the characteristics of star-forming regions in the galaxy.

The points characterizing the color indices of the NGC 5585 ring are located in the two-color diagrams to the left of the NCS (Figs. 8a–8c). The colors of the

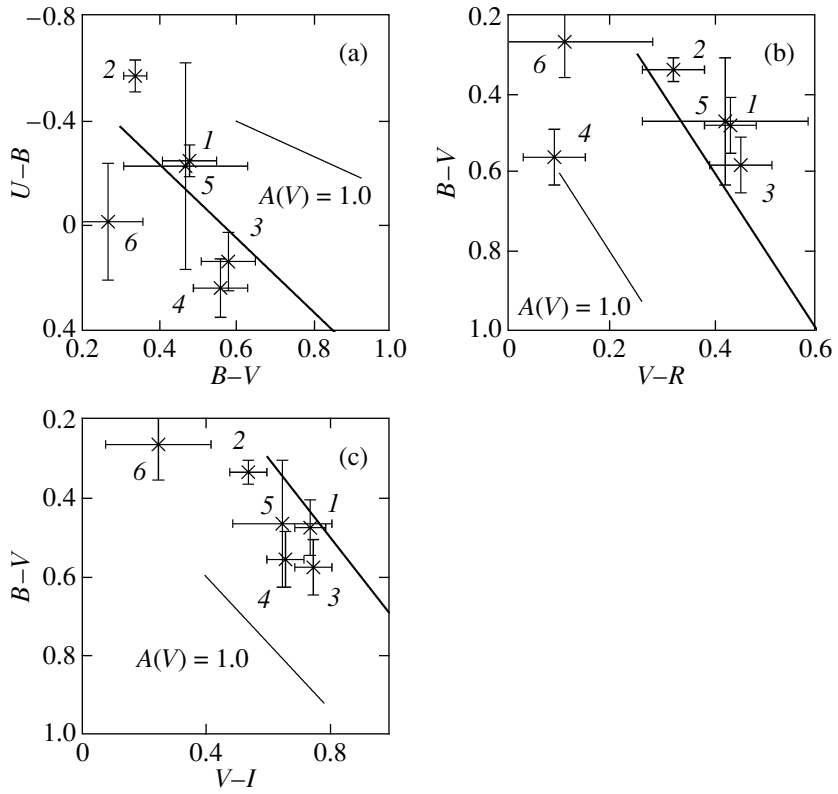

Fig. 8. Positions of the components of the galaxy in two-color diagrams: (a) $(U-B)-(B-V)$, (b) $(B-V)-(V-R)$, and (c) $(B-V)-(V-I)$. For information about the notation, see the text.

ring are characteristic for stellar systems with ongoing active star formation and ages of several Gyrs (i.e., with a small contribution of the old stellar population to the luminosity). The ring is apparently a relatively young structural formation in the galaxy containing numerous regions of current star formation (Fig. 4). The relatively old population of the weak disk is lost against the background of the emission from stars of the NGC 5585 ring.

The old stellar population is often not detected in dwarf galaxies of the Local Group [20]. One of the properties of dwarf galaxies is the burst character of their star formation [21]. In the case of NGC 5585, we observe a "smooth" star-formation history in most of its structural components, as is characteristic of normal galaxies (stellar systems with a burst or bursts of star formation are located far from the NCS in two-color diagrams).

3.5. Regions of Star Formation

We used the "residual" images of NGC 5585 in the U and B bands to identify regions of star formation (Fig. 4). However, although the use of these residual images roughly halves the measurement errors when determining the color indices of the star-forming regions (reducing the error in determining the background around the star-forming region), this approach yields systematic errors associated with inaccuracy in determining the sale for the brightness decrease in the disk in U and I (Table 3). Because of this factor, the difference between the color indices for star-forming regions obtained using the real and residual images of the galaxies increases with distance from the center of NGC 5585. Therefore, we used the real images in the U, B, V, R, and I filters to determine the photometric parameters of the star-forming regions.

To calculate the magnitude of each star-forming region, we constructed a photometric cross section of the region in the B band and determined its full width at half maximum intensity (FWHM). The flux from the star-forming region in each filter was determined within a circular aperture equal to the FWHM of the region along it major axis. The characteristic size of a star-forming region was taken to be equal to the geometric mean of the FWHM along its major and minor axes. We chose a suitable ring for determining the background for each region in the same way (not too small, in order to reduce the error, and not too large, in order to avoid including other regions and structural features in the background). These two parameters were also used to determine the magnitudes of the

star-forming regions in all other filters. We chose the B filter for a number of reasons. The signal-to-noise is higher and the seeing better in the B than in the U filter (Table 2). In addition, the star-forming regions are sometimes much brighter in B than in V, making it possible to reduce the measurement uncertainties. We adopted the FWHM of images of field stars as the uncertainty in the size of a region, which clearly exceeds all other errors. To calculate the ages of the star-forming regions, the derived color indices were plotted on $(U-B)-(B-V)$, $(B-V)-(V-R)$, and $(B-V)-(V-I)$ diagrams on which the evolutionary tracks of various stellar systems computed using the PEGASE2 program were superimposed. To more accurately determine the ages, we used evolutionary tracks computed for metallicities of $Z = 0.008$, 0.02, and 0.05 for models with instantaneous and continuous star formation. Each region was projected onto an evolutionary track along the reddening line. We derived an age interval and the absorption in V using the obtained uncertainties in the color indices. We compared data obtained for the same metallicities, but in different diagrams, choosing values that were common to both intervals. The same procedure was applied for the tracks computed for the different values of Z. In this way, the data were jointly analyzed. A detailed description of this method is presented in [22]. The total uncertainty in the U and R fluxes is determined mainly by uncertainties in the zero point. Note that the PEGASE2 program constructs evolutionary tracks based on model spectra that include emission in both the continuum and lines.

The uncertainty in the characteristic sizes of the star-forming regions taking into account the adopted scales for the images is 43 pc.

A detailed analysis of the parameters of star-forming regions in NGC 5585 is the topic of a separate study, and will be considered in another paper. Here, we present only general information about the characteristics of star-forming regions in the galaxy.

In all, we identified 47 star-forming regions at deprojected distances from the center of 0.1–4.5 kpc (Fig. 4). The characteristic sizes of star-like star-forming regions (i.e., without visible, resolved internal structure) are from 50 to 100 pc, which is the characteristic size of stellar associations (according to the hierarchical classification of Efremov [23]). Identified star-forming regions with visible internal structure (diffuse, multiple, ring-like) have characteristic diameters of 100–180 pc (the sizes of stellar aggregates, according to [23]).

The ages of the star-forming regions in NGC 5585 according to the PEGASE2 models are from 2 to 40 million years, with a maximum in the age distribution at 4–6 million years. Note that star-forming regions located in the NGC 5585 ring are, on average, older than those in the spiral arms of the galaxy.

For essentially all the observed star-forming regions, internal absorption does not exceed 1.5^m in V; for half the regions, $A(V) < 0.5^m$.

We estimate the mean age of the stars in the circumnuclear star-forming region (Fig. 7) to be about four million years for $A(V) = 1.6^m$–1.7^m.

4. DISCUSSION

NGC 5585 has a number of unique properties that set it apart from other similar galaxies. The most important of these are the dominance of dark matter even in inner regions of the galaxy (apart from the circumnuclear region); the presence of numerous star-forming regions, although molecular hydrogen has not been detected in the galaxy; the absence of structural components dominated by an old stellar population (the bulge of NGC 5585 is the reddest region of the galaxy, and its color indices, Sersic parameter and relative dimensions are more similar to those of an inner disk); the asymmetry of the galaxy structure; and the presence of a region of current star formation 100 pc from the galactic nucleus.

Let us consider in more detail the morphology of NGC 5585 and star-forming processes in the galaxy. The spiral arms appear to be "residual" structures that are wound in opposite directions. This type of arm in a galaxy such as NGC 5585 could be taken to be a bar. Bars whose centers do not coincide with the center of their galaxies can indeed form in late-type galaxies with low-mass disks (for example, in the LMC) [24] (note that the dynamical and photometric centers of NGC 5585 do coincide). However, dynamical models show that such bar-like, non-centrally-symmetrical structures form when the contribution of a dark, spherical halo is small or absent [24]. We have the opposite case in NGC 5585. Based on the above, in our opinion, we do not observe a bar in NGC 5585: neither the southwestern nor the weaker southern arms (P.A. = 20°, Fig. 4) can form the southern part of a bar, since the northern spiral arm has a somewhat different position angle and appreciable curvature. Therefore, we are inclined to agree with the conclusion of [3] that there is no bar in NGC 5585.

The deficit of molecular hydrogen (or more precisely, the low flux in the CO line) in the presence of active star formation is not unique among low-surface-brightness galaxies [25]. This may be associated with a real deficit of H_2, or uncertainty in the coefficient for translating $I(\mathrm{CO})$ into $M(\mathrm{H_2})$ due to the low density and low metallicity of the gas [25]. At the same time, NGC 5585 is one of the bluest galaxies in its class, and star formation has actively occurred

and remains ongoing in this galaxy. While star formation in the bulge and disk proceed according to the law that is usual for disks (with the star-forming intensity varying smoothly with time and being roughly proportional to the amount of gas in the given region), the star-formation rate in the nucleus and spiral arms has remained virtually constant in time (as we can conclude from their positions in two-color diagrams). This means that either the efficiency of star formation has increased in time in these regions or there is a constant input of gas to the nucleus and spiral arms of the galaxy. Note as well the presence of a ring whose age does not exceed several Gyrs, forming the youngest structure in the galaxy.

Currently, star formation is actively occurring in the spiral arms and ring of NGC 5585, and also in circumnuclear regions. One result is the presence of numerous star-forming regions and supernova remnants in the galaxy (according to [8]).

The collected data on the structure (form of the spiral arms; the ring, whose center does not coincide with the galactic center) and star-forming processes in the galaxy may indicate that NGC 5585 formed as a result of a merger of two galaxies, or that it absorbed one or several small satellite galaxies during its evolution. Judging from the age of the ring, such an event may have occurred several Gyrs ago.

Supporting (or rejecting) this hypothesis requires additional study, first and foremost, obtaining a two-dimensional map of the velocities in the circumnuclear region and in the region to the north of the galactic nucleus (at the intersection of the northern and southwestern spiral arms). It would be valuable to carry out dynamical modeling in order to estimate the initial parameters of galaxies participating in the purported merger (absorption) that would yield a stellar system whose structure is close to that of NGC 5585.

5. CONCLUSIONS

1. We have carried out the first five-color surface photometry of NGC 5585 in order to study the structure of the galaxy and the composition of its stellar population.

2. Based on our two-dimensional decomposition, both components of the galaxy—the disk and bulge (with Sersic parameter $n = 1.2–1.6$)—have reduced surface brightness. In the transition from short- to long-wavelength bands, the scale length of the disk and the effective radius of the bulge decrease, as well as the Sersic parameter. The scale length of the disk and the effective radius of the bulge are the same in the R and I bands, and equal to $30''–40''$ (0.8–1.1 kpc).

3. NGC 5585 possesses a (pseudo) bar and ring. However, the center of the bar-like structure, ring, and galaxy do not coincide. The spiral arms of the galaxy appear to be wound in opposite directions.

4. The star-formation history of NGC 5585 is typical for late-type spiral galaxies: star formation proceeds fairly actively and smoothly, without powerful star-formation bursts. There is no old stellar population in the ring of the galaxy (with ages of the order of 10 Gyrs). The photometric characteristics of the NGC 5585 bulge—the reddest region of the galaxy—are typical for the disks of spiral galaxies.

5. A powerful star-forming region with an age of about four million years is located $3.2''$ (100 pc) from the center of the galaxy, whose emission swamps the nucleus in the U and B bands.

6. Forty-seven star-forming regions have been identified in the galaxy, with sizes from 50 to 180 pc and ages not exceeding 40 million years.

ACKNOWLEDGMENTS

The authors thank O.V. Ezhkova, A.V. Zasov, and E.V. Shimanovskaya (Sternberg Astronomical Institute) for their help, valuable advice, and consultation. This work was supported by the Russian Foundation for Basic Research (project nos. 07-02-00792 and 08-02-01323).

REFERENCES

1. M. Spano, M. Marcelin, P. Amram, et al., Mon. Not. R. Astron. Soc. **383**, 297 (2008).
2. H. M. Hernandez-Toledo and S. Ortega-Esbri, Astron. Astrophys. **487**, 485 (2008).
3. K. Menendez-Delmestre, K. Sheth, E. Schinnerer, et al., Astrophys. J. **657**, 790 (2007).
4. A. Seth, M. Agueros, D. Lee, and A. Basu-Zych, Astrophys. J. **678**, 116 (2008).
5. R. C. Kennicutt, Jr., Astrophys. J. **334**, 144 (1988).
6. A. Alonso-Herrero and J. H. Knapen, Astron. J. **122**, 1350 (2001).
7. S. S. Larsen, Astron. Astrophys. **416**, 537 (2004).
8. D. M. Matonick and R. A. Fesen, Astrophys. J. Suppl. Ser. **112**, 49 (1997).
9. M. Das, K. O'Neil, S. N. Vogel, and S. McGaugh, Astrophys. J. **651**, 853 (2006).
10. S. Blais-Ouellette, C. Carignan, P. Amram, and S. Cote, Astron. J. **118**, 2123 (1999).
11. I. D. Karachentsev, V. E. Karachentseva, W. K. Huchtmeier, and D. I. Makarov, Astron. J. **127**, 2031 (2004).
12. G. Fabbiano and N. Panagia, Astrophys. J. **266**, 568 (1983).
13. S. Cote, C. Carignan, and R. Sancisi, Astron. J. **102**, 904 (1991).
14. A. U. Landolt, Astron. J. **104**, 340 (1992).
15. C. Y. Peng, L. C. Ho, C. D. Impey, and H.-W. Rix, Astron. J. **124**, 266 (2002).

16. P. J. Grosbol, Astron. Astrophys. Suppl. Ser. **60**, 261 (1985).
17. A. S. Gusev, Astron. Zh. **84**, 3 (2007) [Astron. Rep. **51**, 1 (2007)].
18. C. Mollenhoff, Astron. Astrophys. **415**, 63 (2004).
19. R. Buta and K. L. Williams, Astron. J. **109**, 543 (1995).
20. S. van den Bergh, *The Galaxies of the Local Group* (Cambridge Univ., Cambridge, 2000).
21. E. K. Grebel, in *Star Formation from the Small to the Large Scale,* ESTEC, Ed. by F. Favata, A. A. Kaas, and A. Wilson, ESA SP-445 (Eur. Space Agency, 2000), p. 87.
22. A. S. Gusev and M.-G. Park, Astron. Astrophys. **410**, 117 (2003).
23. Yu. N. Efremov, *Star Formation Centers in Galaxies* (Nauka, Moscow, 1989) [in Russian].
24. A. V. Zasov and A. V. Khoperskov, Astron. Zh. **79**, 195 (2002) [Astron. Rep. **46**, 173 (2002)].
25. L. D. Matthews, Y. Gao, J. M. Uson, and F. Combes, Astron. J. **129**, 1849 (2005).

Translated by D. Gabuzda